BIOCHEMISTRY
including biophysical chemistry & molecular biology

Article

pubs.acs.org/biochemistry

Controlling Conformational Flexibility of an O_2-Binding H-NOX Domain

Emily E. Weinert,[†,∥] Christine M. Phillips-Piro,[†,∥] Rosalie Tran,[†,§] Richard A. Mathies,[†] and Michael A. Marletta*[,†,‡]

[†]Department of Chemistry and [‡]Molecular and Cell Biology, University of California, Berkeley, Berkeley, California 94720, United States

Supporting Information

ABSTRACT: *H*eme *N*itric oxide/*OX*ygen binding (H-NOX) domains have provided a novel scaffold to probe ligand affinity in hemoproteins. Mutation of isoleucine 5, a conserved residue located in the heme-binding pocket of the H-NOX domain from *Thermoanaerobacter tengcongensis* (*Tt* H-NOX), was carried out to examine changes in oxygen (O_2)-binding properties. A series of I5 mutants (I5F, I5F/I75F, I5F/L144F, I5F/I75F/L144F) were investigated to probe the role of steric bulk within the heme pocket. The mutations significantly increased O_2 association rates (1.5−2.5-fold) and dissociation rates (8−190-fold) as compared to wild-type *Tt* H-NOX. Structural changes that accompanied the I5F mutation were characterized using X-ray crystallography and resonance Raman spectroscopy. A 1.67 Å crystal structure of the I5F mutant indicated that introducing a phenylalanine at position 5 resulted in a significant shift of the N-terminal domain of the protein, causing an opening of the heme pocket. This movement also resulted in an increased amount of flexibility at the N-terminus and the loop covering the N-terminal helix as indicated by the two conformations of the first six N-terminal amino acids, high *B*-factors in this region of the protein, and partially discontinuous electron density. In addition, introduction of a phenylalanine at position 5 resulted in increased flexibility of the heme within the pocket and weakened hydrogen bonding to the bound O_2 as measured by resonance Raman spectroscopy. This study provides insight into the critical role of I5 in controlling conformational flexibility and ligand affinity in H-NOX proteins.

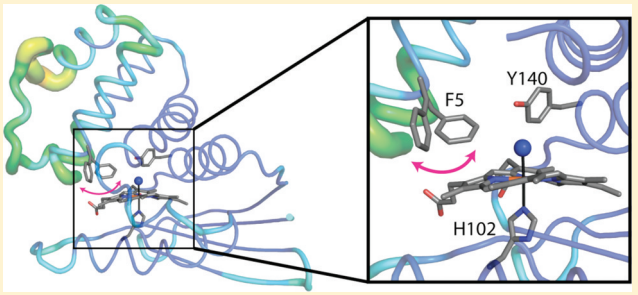

Hemoproteins are involved in many crucial cellular processes, including oxidative transformations (P450s), O_2 delivery and transport [myoglobin (Mb), hemoglobin (Hb)], and diatomic gas signaling [soluble guanylate cyclase (sGC), CooA]. Attempts to understand the factors that control reactivity versus reversible ligand binding in heme proteins have been the subject of intense study for many decades. While some causes of differences in reactivity are more straightforward, such as thiolate- versus histidyl-ligated hemes, the method by which a protein controls the reactivity of the iron and reversible ligand binding is not fully understood. The majority of the previous work undertaken to elucidate factors responsible for ligand affinity and selectivity in reversible O_2-binding heme proteins has been performed on proteins with a globin fold, primarily myoglobin (Mb)[1,2] and hemoglobin (Hb).[3,4] These studies on the globins have provided a wealth of information as to how the globin fold modulates ligand affinity and O_2 reactivity. Through this work, it has become apparent that many factors affect ligand affinity, including the distal ligand, heme pocket polarity, off-heme binding sites, and iron−histidine bond strength.[1,2,5−7] Understanding all of the factors involved in controlling ligand binding within heme proteins should allow for the rational engineering of novel proteins for a variety of biotechnological and biomedical applications. However, whether the factors controlling O_2 binding within globin domains are specific to this fold or are universal to all heme protein folds has only begun to be investigated.

The recent discovery of a new class of heme proteins, termed *H*eme *N*itric oxide/*OX*ygen (H-NOX) binding domains,[8,9] has provided additional insight into how heme proteins control ligand affinity. Soluble guanylate cyclase (sGC), the mammalian receptor for nitric oxide (NO), which regulates functions as diverse as vasodilation, neuropotentiation, and egg fertilization, contains an H-NOX domain that slectively senses NO.[10] To date, H-NOX domains from mammalian sGCs and aerobic bacteria do not form stable complexes with O_2, either by limiting access of O_2 to the heme or by tuning the heme pocket such that O_2 binding is extremely unfavorable.[11−13] In contrast, H-NOX domains characterized from anaerobic bacteria, such as *T. tengcongensis*, have been found to tightly bind O_2 (K_d ∼ 48 nM) [ref 11; EEW and MAM, unpublished data]. Structures of both O_2- and non-O_2-binding H-NOX proteins exhibit the same protein fold (Figure 1, rmsd 1.88 Å[14,15]), making this class of proteins ideal for dissecting the factors that allow a single protein fold to exhibit widely varying ligand affinities and

Received: May 20, 2011
Revised: June 21, 2011
Published: July 3, 2011

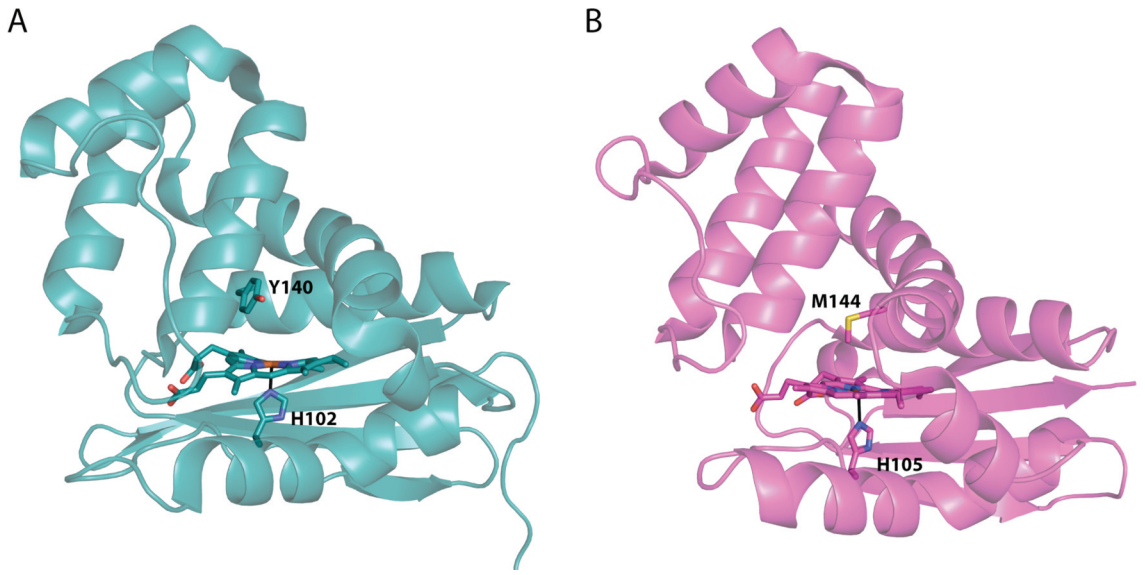

Figure 1. Structures of the (A) O_2-binding WT *Tt* H-NOX (1U55, chain A) in teal[15] and (B) a non-O_2-binding H-NOX from *Nostoc sp* in magenta.[14] Hemes and coordinating histidines, as well as the distal pocket residue above the heme, are shown in sticks. A global alignment of these two structures results in an rmsd of 1.88 Å (using C_α−C_α).

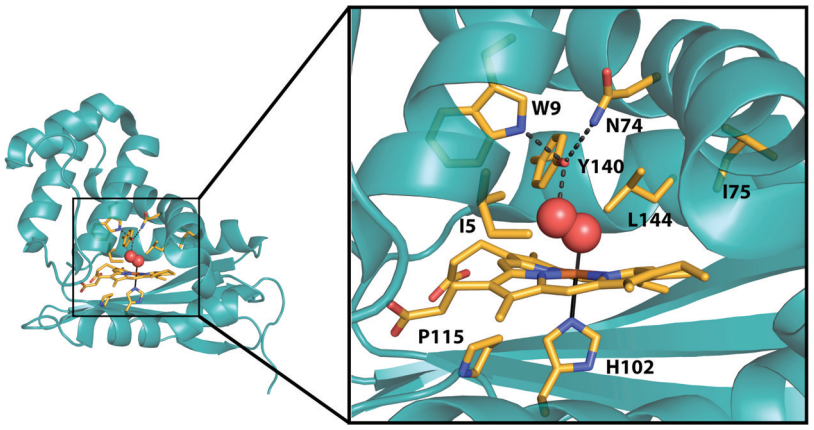

Figure 2. Key residue side chains and the heme within the *Tt* H-NOX heme pocket are shown in stick representation with carbon atoms in orange, oxygens in red, and nitrogens in blue using chain A of PDB 1U55.[15]

specificities. In addition, as *Tt* H-NOX is amenable to mutagenesis[11,16−18] and exhibits a fold that is structurally distinct from the globins (Figure S1), it provides a useful model for probing the effects of various mutations on ligand affinity and reactivity, as well as identifying factors that are independent of protein fold.

Previous mutational studies on H-NOX domains[11,16,18] have found that the presence of hydrogen-bonding residues within the distal pocket is a major determinant of O_2-binding (Figure 2).[15] In *Tt* H-NOX, the hydrogen-bonding triad consists of Y140, which directly forms a hydrogen bond to the bound O_2, as well as W9 and N74, which orient Y140 within the binding pocket via H-bonds. Removal of Y140 results in diminished O_2 affinity (Y140L), while mutation of both Y140 and W9 results in a *Tt* H-NOX mutant with no measurable O_2 binding (Y140L/W9F).[11] Conversely, introduction of hydrogen bond donors into the distal heme pocket of full length sGC does not result in stable O_2 binding,[19,20] suggesting that there are factors in addition to hydrogen bonding involved in controlling reversible O_2 binding in H-NOX domains.

Another feature of H-NOX domains that affects ligand affinity is the highly distorted heme cofactor.[15] Flattening the heme, through mutation of P115 (P115A), resulted in increased O_2 affinity.[16] This increased affinity was attributed to a change in the tilt of the proximal histidine, allowing for increased orbital overlap between the O_2 and heme iron thereby strengthening the Fe−O_2 bond.[16] In addition, introduction of steric bulk in the form of phenylalanine residues to the heme distal pocket of *Tt* H-NOX, analogous to the phenylalanine found within the sGC heme pocket,[2] was found to rearrange the heme pocket (I75F/L144F).[18] Interestingly, the heme in the I75F/L144F mutant was found to be flatter than in WT *Tt* H-NOX, similar to the P115A mutant; however, unlike the P115A mutant, the oxygen affinity decreased in the I75F/L144F mutant.[18] Thus, many factors control ligand affinity and selectivity within the H-NOX family, and further studies are necessary to fully understand how each of these factors contribute to produce a finely tuned O_2 binding protein.

In this work, we examined the effect of increased steric bulk and structural flexibility in the distal pocket of *Tt* H-NOX on O_2-binding properties and kinetics. The I5 position was chosen for mutagenesis because a medium-sized, hydrophobic amino

dx.doi.org/10.1021/bi200788x | *Biochemistry* 2011, 50, 6832−6840

acid (I, L, V) is highly conserved and within van der Waals contact with the heme (Figure 2), suggesting an important role in controlling ligand affinity and protein structure. Changes in protein structure and ligand binding were investigated in a panel of I5 mutations using time-resolved UV−vis spectroscopy, X-ray crystallography, and steady-state resonance Raman spectroscopy. In addition, the interplay between the I5F mutation and the previously described I75F, L144F, and I75F/L144F mutations was investigated. Together these data point to the critical role of I5 in controlling flexibility and ligand affinity within the H-NOX family.

MATERIALS AND METHODS

Materials and General Methods. Unless otherwise noted, all reagents were purchased in the highest available purity and used as received.

Protein Expression and Purification. Expressions and purifications of H-NOX proteins were performed as previously described.[18] Briefly, cultures were grown at 37 °C to an OD_{600} of 0.6−1 in media (45 g of yeast extract, 1.6 g of KH_2PO_4, 11.5 g of $K_2HPO_4{\cdot}3H_2O$, 1.3% glycerol per 1 L) and cooled to 18 °C prior to induction. Isopropyl β-D-thiogalactopyranoside (Research Products International Corp.) was added to 10 μM, and aminolevulinic acid (Cosmo Bio Co. Ltd.) was added to 1 mM. Cultures were grown overnight for 18−24 h and then harvested. Cells were lysed using a homogenizer in 50 mM TEA (pH 7.5), 300 mM NaCl, 10 mM imidazole (buffer A) with Pefabloc (Centerchem Inc.), and benzamidine (Sigma-Aldrich) added to 1 mM. Lysates were heat-denatured at 70 °C for 40 min and then pelleted at 130000*g*. Supernatants were applied to HisPure columns (Pierce) pre-equilibrated with buffer A. The protein-loaded columns were then washed with 25−30 column volumes of buffer A. H-NOX proteins were eluted in buffer A containing 150 mM imidazole and concentrated to <2 mL. The proteins were then desalted into 50 mM TEA (pH 7.5), 20 mM NaCl, 5% glycerol (buffer B) using PD10 columns (GE Lifesciences) and stored at −80 °C.

UV−vis Spectroscopy. All spectra were recorded on either a Cary 3E spectrophotometer equipped with a Neslab RTE-100 constant temperature bath or a Cary 300Bio spectrophotometer equipped with a Peltier accessory. Preparation of complexes was carried out in buffer B as previously described.[9,11,18]

O_2 Dissociation Rate. O_2 dissociation rate experiments were performed as previously described with the following modifications.[11,18] Protein and dithionite traps were prepared in buffer B and saturating CO was not used as part of the trap due to a rate dependence on CO concentration. Dithionite concentration did not affect the O_2 dissociation rate. The dissociation of O_2 from the heme was monitored and fit globally using SpecFit32 (HiTech Scientific).[11,18]

O_2 Association Rate. O_2 association to the heme was observed using flash photolysis and transient absorption spectroscopy as previously described.[18] Briefly, the Fe^{II}−CO complex was generated in an anaerobic chamber, as described in an earlier publication,[11] and diluted to ∼8 μM with anaerobic buffer in a 1 cm path length quartz cuvette. The Fe−CO bond was photolyzed by excitation with 8 ns pulses of 532 nm from a doubled Nd:YAG laser, using an apparatus described elsewhere.[21] The cuvette was opened to air and stirred with a steady stream of air blown into the mouth of the cuvette to fully saturate the solution for measurement of the O_2 association rates. Spectra were taken at ∼20 °C. Data points were collected at a rate of 1×10^9 s^{-1} using a LeCroy digital oscilloscope.

Purification of Untagged I5F *Tt* H-NOX for Crystallization. Non-His_6-tagged I5F *Tt* H-NOX was expressed as described above. Cells were resuspended in 50 mM TEA (pH 7.5), 50 mM NaCl and were lysed by passage through a homogenizer at 10000 psi. The lysate was heat-denatured at 70 °C for 40 min and pelleted at 130000*g*. The supernatant was passed over a SuperQ-650 M anion-exchange column (Toyopearl), and the flow-through was collected. The flow-through was buffer exchanged into 50 mM HEPES (pH 6.5), 5% glycerol using a G25 size exclusion column and then loaded onto a CM-650 M cation-exchange column (Toyopearl). Protein was eluted using a linear gradient from 0−500 mM NaCl. Fractions containing the highest purity H-NOX protein were pooled and passed over a S75 16/60 size-exclusion column (Pharmacia) that had been equilibrated with buffer B. Only fractions containing H-NOX protein with a ratio of $A_{417\ nm}/A_{280\ nm} > 1.6$ were pooled, concentrated, and flash-frozen in liquid nitrogen for storage at −80 °C.

Crystal Structure of I5F *Tt* H-NOX. As-purified non-His-tagged I5F *Tt* H-NOX protein was thawed, buffer exchanged into 20 mM TEA (pH 7.5) using a PD-10 column, and then concentrated to 26 mg/mL. The protein was crystallized via sitting drop vaper diffusion by mixing 1 μL of protein with 1 μL of precipitant solution (0.2 M ammonium sulfate, 20% PEG 3350) and equilibrating the drop against 400 μL of precipitant. Crystals formed within 2 days and were cryoprotected by a brief soak in well solution containing 25% ethylene glycol and then frozen in liquid nitrogen for storage.

X-ray diffraction data were collected at the Advanced Light Source (ALS) at Lawrence Berkeley National Laboratory (Berkeley, CA) on beamline 5.0.1 (λ = 0.977408 Å). Crystals diffracted to 1.67 Å and data were processed in HKL2000[22] with space group $P2_1$.

The protein crystallized with two protein monomers in the asymmetric unit. The protein component (heme and water molecules removed) of the WT structure (PDB ID 1U55) was used for molecular replacement in PHASER.[23] The resulting structure was refined in Phenix[24] against 1.67 Å data with alternate cycles of positional and ADP refinement with manual refitting in Coot.[25] A TLS model was incorporated toward the end of refinement. The final model contains 2 chains with 185 residues in chain A and 183 residues in chain B. 153 water molecules and two heme molecules were also modeled to produce the final refinement parameters of R_{work} of 19.7% and R_{free} of 24.7%.

Resonance Raman Spectroscopy. Fe^{II}−O_2 *Tt* H-NOX samples were prepared and all spectra were acquired as previously described.[9,26]

RESULTS AND DISCUSSION

Spectroscopic and Kinetic Effects of the I5F Mutation. To determine how mutation of I5 affects ligand affinity in *Tt* H-NOX, the O_2 binding properties of the leucine and phenylalanine mutants were investigated with steady-state and time-resolved UV−vis spectroscopy. In addition to the I5L and I5F single mutants, the I5F mutation was introduced in combination with the previously described I75F, L144F, and I75F/L144F mutants[26] to probe the role of distal pocket steric bulk. This resulted in the following panel of I5F *Tt* H-NOX mutants: I5F, I5F/I75F, I5F/L144F, and I5F/I75F/L144F. The

Table 1. Kinetic Constants for Ligand Binding to *Tt* H-NOX Domains

Tt H-NOX	K_d O_2 (nM)	k_{off} O_2 (s^{-1})	k_{on} O_2 (μM^{-1} s^{-1})
WT	48 ± 5	1.20 ± 0.02[a,b]	25 ± 3
I75F	497 ± 16[b]	11.19 ± 0.12[b]	22.5 ± 0.7[b]
L144F	2360 ± 50[b]	16.06 ± 0.21[b]	6.8 ± 0.1[b]
I75F/L144F	11150 ± 330[b]	45.7 ± 0.9[b]	4.1 ± 0.1[b]
I5L	413 ± 33	9.50 ± 0.64	23 ± 1
I5F	1570 ± 50	61.3 ± 1.5	39.0 ± 0.5
I5F/I75F	3730 ± 150	233 ± 10	62.5 ± 0.1
I5F/L144F	3750 ± 110	39.0 ± 0.8	10.4 ± 0.2
I5F/I75F/L144F	3160 ± 380	60.9 ± 7.1	19.3 ± 0.2

[a]Reference 11. [b]Reference 18.

steady−state UV−vis spectra of the mutants were very similar to the wild-type protein. As the number of phenylalanine residues within the distal pocket increased, a small shift toward longer wavelengths was observed in the Soret absorbance maximum, with a concomitant shift of the α/β bands toward shorter wavelengths, which is potentially due to a structural change within the heme pocket. In addition, a mixture of 5- and 6-coordinate Fe^{II}−NO complexes was observed for most of the mutants, as was previously described for the I75F, L144F, and I75F/L144F mutants (Table S1). However, two exceptions to this observed 5/6-coordinate mixture were the I5L[26] and I5F single mutants, which were exclusively 6-coordinate. This suggests that changes to the heme electronics and structure differ when steric bulk is added at the I5 versus the I75 and L144 positions, which are on the opposite side of the *Tt* H-NOX heme pocket (Figure 2).

The kinetics of O_2 binding were investigated to determine the effect of adding steric bulk at the I5 position as well as the effect of additional bulk at positions 75 and 144. It was previously found that introduction of phenylalanine residues at positions 75 and 144 resulted in weaker O_2 affinities.[18] The I75F, L144F, and I75F/L144F mutants all exhibited faster O_2 dissociation rates, while the L144F and I75F/L144F mutations resulted in slower O_2 association rates. This had a net effect of significantly decreasing the O_2 affinities (10−230-fold) for all of the I75 and L144 mutants (Table 1).

In the present work, the conservative I5L mutation did not affect the O_2 association rate, (23 μM^{-1} s^{-1}, compared to 22 μM^{-1} s^{-1} for WT); however, the O_2 dissociation rate increased to 9.5 s^{-1}, as compared to 1.20 s^{-1} for WT (Table 1 and Figure 3). Upon introduction of the bulkier I5F mutation, the O_2 association and dissociation rates increased to 39 μM^{-1} s^{-1} and 61.3 s^{-1}, respectively (Table 1 and Figure 3). An O_2 dissociation rate of 61.3 s^{-1} is extremely fast for *Tt* H-NOX, suggesting that these mutations may open the heme pocket to increase both ligand accessibility and dissociation. A more accessible and/or flexibile heme pocket is also consistent with the NO dissociation rate data (Table S2). The I5F mutant was the only mutant to exhibit monoexponential NO dissociation rates. This may be due to altered dynamics of the I5F mutant that allows more facile entry and exit of ligands from the heme pocket or through cavities within the protein [Winter, M., Herzik, M., and Marletta, M. A., unpublished results].

In addition to the single I5 mutations, the panel of double and triple mutants was also investigated to determine how increased bulk at both ends of the distal pocket affects O_2 binding kinetics. The I5F mutation was found to synergize with

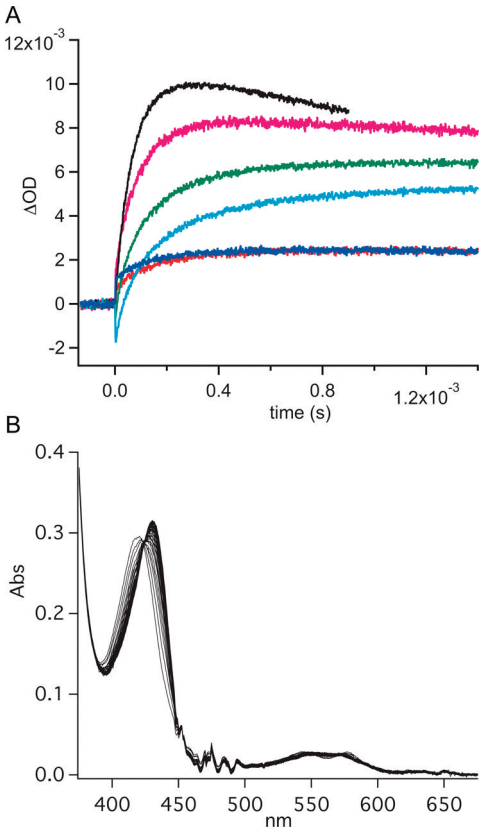

Figure 3. Laser photolysis traces of the photolysis of the Fe^{II}−CO complex followed by binding of O_2 (A), and representative stopped flow kinetic data (B). WT in red; I5L in blue; I5F/L144F in teal; I5F/I75F/L144F in green; I5F in magenta; I5F/I75F in black. Laser photolysis data were analyzed using Igor Pro. Stopped flow data were analyzed using SpecFit32.

the I75F, L144F, and I75F/L144F mutants—in each case resulting in faster O_2 association and dissociation rates—when compared to the parent proteins. Of these double and triple mutants, the I5F/I75F mutant was found to have by far the greatest changes in O_2 kinetics, exhibiting the fastest O_2 association and dissociation rates measured for an H-NOX protein thus far (62.5 μM^{-1} s^{-1} and 233 s^{-1}, respectively, Table 1 and Figure 3). These rates correspond to a 3-fold increase in association rate and a 195-fold increase in dissociation rate for O_2 as compared to WT *Tt* H-NOX. Therefore, it is likely that the changes to the protein flexibility and/or structure differed between the double mutants, resulting in the varied ligand binding kinetics.

X-ray Crystal Structure of the I5F Mutant. A structure of the conservative I5L mutant has previously been described, and only small differences were found when compared with the WT *Tt* H-NOX structure with a global C_α−C_α rmsd of 0.34 Å (Figure 4A).[17] A slight rotation of the N-terminal subdomain relative to the C-terminal subdomain was observed, as was a small relaxation of the heme distortion. These differences between the WT and I5L structures are likely the cause of the modest changes in the O_2 binding kinetics.

The structure of the sterically bulky I5F mutant was solved to investigate how the mutation caused the markedly increased O_2 binding kinetics. A 1.67 Å resolution crystal structure of the mutant indicates that the overall structure of the I5F mutant retains the H-NOX fold (Figure 4B). A well-ordered water

dx.doi.org/10.1021/bi200788x | *Biochemistry* 2011, 50, 6832−6840

molecule is bound above the heme, illustrating that the protein crystallized in the $Fe^{III}-H_2O$ state. Alignment of the last 80 C-terminal residues of the I5F and WT structures produced the lowest overall rmsd of 1.13 Å and illustrates that the most notable change introduced by the addition of the I5F mutation is the movement of the N-terminal domain with respect to the C-terminal domain (Figure 4B). The displacement of the N-terminal region of the structure can be traced to increased bulk and two conformations of the phenylalanine at position 5. The two conformations of the phenylalanine result in disorder of the first six residues at the N-terminus, which have also been modeled in two conformations (Figure 5). While the two conformations of the F5 residue are clearly represented in a composite omit map, the remaining residues at the N-terminus are less clearly located in the density and suggest an increased amount of disorder in this region of the structure (Figure 5). The amount of disorder in the N-terminal region indicates that this region is flexible and likely dynamic in solution.

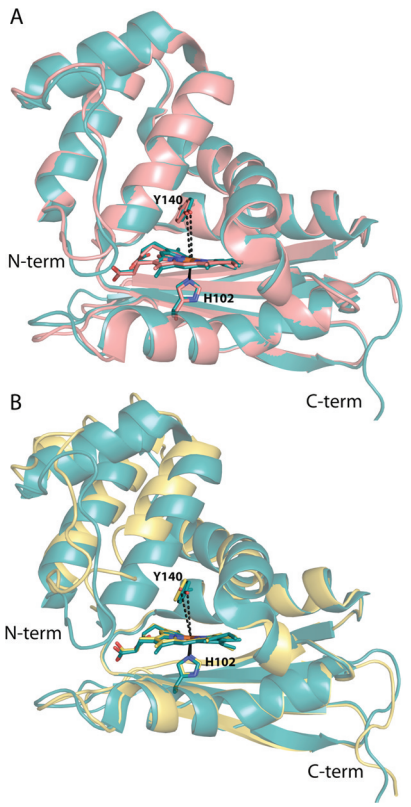

Figure 4. Structural alignments of the WT *Tt* H-NOX structure with the I5L and I5F mutant structures. (A) Global alignment of WT (teal, PDB ID 1U55)[15] and I5L (salmon, PDB ID 3NVR)[17] *Tt* H-NOX structures; rmsd 0.34 Å. The Y140–Fe distances are shown in dashed black lines and are 5.0 and 5.1 Å in the WT and I5L structures, respectively. (B) Overlays of the WT (teal, PDB ID 1U55)[15] and I5F (yellow) mutant structures shown following alignment of the last 80 amino acids (C-terminus) of the proteins; rmsd 1.13 Å. The Y140–Fe distances are shown in black dashed lines with the I5F distance being 5.6 Å. H102, Y140, and the heme are shown in sticks for orientation.

In all previously determined *Tt* H-NOX structures, the N-terminus is well ordered and clearly present in a single conformation. Thus, the increased flexibility in this region of the structure, which directly covers the heme pocket, allows for greater access to the heme pocket and likely contributes to the rapid O_2 association and dissociation rates. In addition to the disorder seen at the N-terminus, the loop covering the N-terminal helix (residues 27–47) is also highly disordered with discontinuous backbone density (Supporting Information Figure S3) and increased *B*-factors with respect to the rest of the structure (49 $Å^2$ vs 26 $Å^2$; Figure 6). These observations are again consistent with a more dynamic protein with rapid ligand flux in and out of the heme pocket. Phenylalanine 78 lies above the heme on the opposite side of the pocket from F5 and like F5 is in two conformations in the pocket (Supporting Information Figure S4). The two conformations of F78 are suggestive of increased flexibility within the heme pocket.

In addition to the disorder at the N-terminus, the Y140–Fe distance was also lengthened, from 5.0 Å for WT (either $Fe^{II}-O_2$ or $Fe^{III}-H_2O$ structures) to 5.6 Å for the $Fe^{III}-H_2O$ I5F mutant (Figure 4B). It was previously found that increasing the distance between the distal pocket hydrogen bond donor and the iron results in a weaker hydrogen bond to the bound O_2 and subsequent reduction in O_2 affinity.[18] The pocket volume has increased slightly due to the N-terminal shift away from the heme and protein core. The increased flexbility and opening of the heme pocket, in concert with the increased Y140–Fe distance, likely results in decreased ligand trapping at the heme, contributing to the decreased O_2 affinity of the I5F mutant.

Resonance Raman Characterization of I5F Heme Flexibility. To further investigate how introduction of the I5F mutation changes the local heme environment, steady-state resonance Raman (RR) spectra of the $Fe^{II}-O_2$ protein were obtained. Previous work has found that the conformation of the heme and protein are intricately linked,[12,15] suggesting that the multiple confomers of the protein are most likely

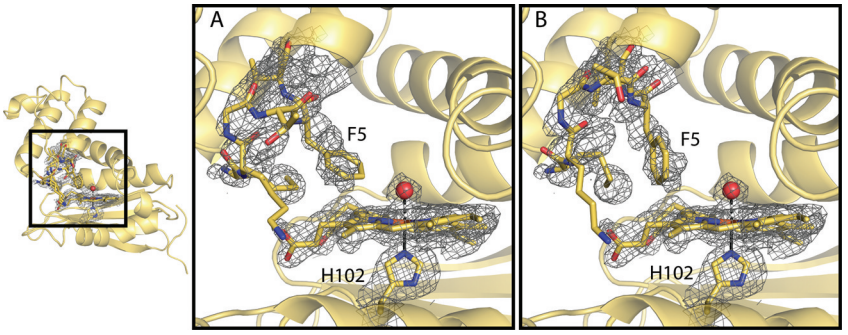

Figure 5. Heme cofactor and disordered N-terminus of the I5F *Tt* H-NOX structure. Composite omit map at 1.0 σ indicating two conformations (A, B) of the first six N-terminal residues. Residues 1–6 are shown in sticks with yellow carbon, red oxygen, and blue nitrogen atoms. The heme cofactor, coordinating water molecule, and coordinating histidine 102 are also shown in sticks and with corresponding composite omit density for comparison.

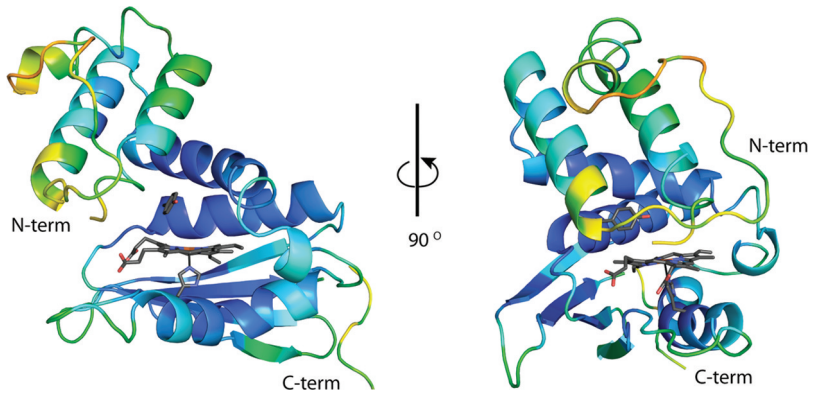

Figure 6. I5F *Tt* H-NOX colored in rainbow by *B*-factor. The areas of the structure with the highest *B*-factors (70 Å^2) are in red and the lowest *B*-factors (10 Å^2) in dark blue. The heme, Y140, and H102 are shown in gray sticks for orientation.

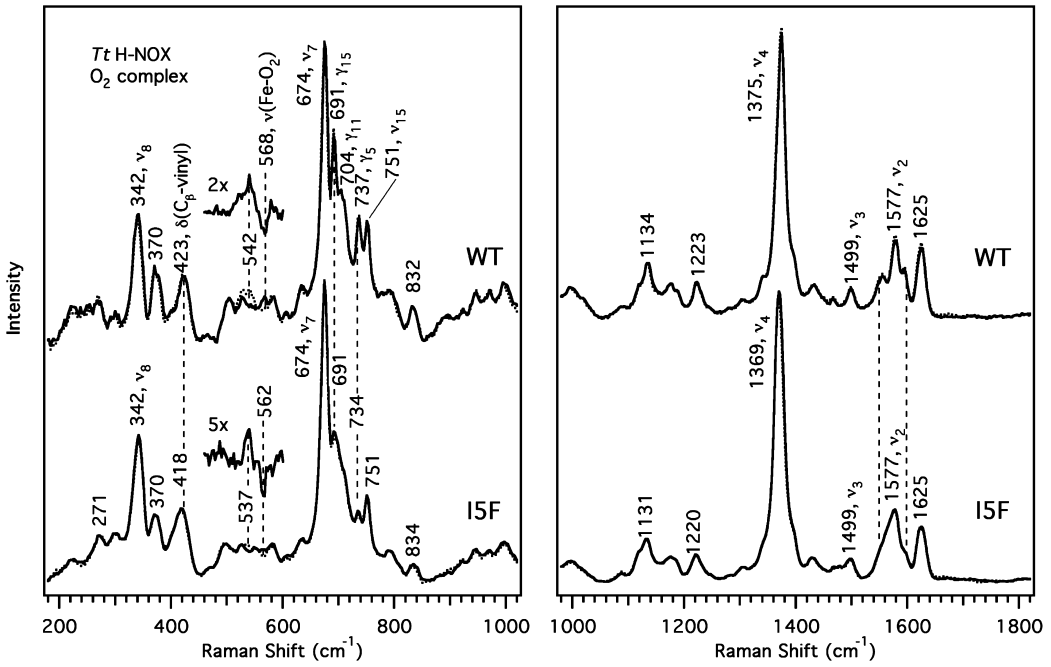

Figure 7. Resonance Raman spectra of the O_2 complexes of WT and I5F *Tt* H-NOX. $^{18}O_2$ spectra (dotted trace) are overlapped with the $^{16}O_2$ spectra to indicate the frequency shifts upon isotopic substitution. Difference ($^{18}O_2 - {}^{16}O_2$) spectra are magnified and overlaid above each protein for clarity. Spectral intensities were normalized to ν_7 and ν_4 for the low and high frequencies, respectively.

transmitted into additional flexibility of the heme. Resonance Raman spectroscopy is highly sensitive to changes in the heme environment and structure, providing detailed information about the changes introduced by the mutations in solution.[27−30] The main heme skeletal markers in the high-frequency region can be used to assess differences in the heme macrocycle core size (ν_4) and conformation (ν_3, ν_2, and ν_{10}), in addition to the spin and coordination states. Furthermore, heme deformation modes (e.g., $\delta(C_\beta$-vinyl), γ_{15}, ν_8) and the $Fe^{II}-O_2$ stretching mode in the low-frequency region can reveal details about the heme structure and $Fe^{II}-O_2$ bond strength.

Previous characterizations of the I5L mutant by UV−vis and RR spectroscopy[26] illustrate that the I5L protein has very few spectral differences with comparison to WT *Tt* H-NOX[9] (Table S3). However, there were some broadened heme skeletal modes and slight decreases in the RR intensity of heme out-of-plane modes in the RR spectra. These features demonstrate that there is some overall conformational flexibility and a slight relaxation toward a more planar geometry of the heme in the I5L mutant.[26]

When compared to WT *Tt* H-NOX, the heme vibrational modes of the I5F mutant were found at the same frequencies as in the WT spectra but were considerably broadened, suggesting markedly increased flexibility (Figure 7 and Table S3).[9,26] In addition, the low-frequency heme out-of-plane modes were also evident in the RR spectra, albeit at slightly reduced intensities compared to the WT protein. Therefore, the heme deformation observed for the WT protein in the RR spectra and crystal structures is likely conserved in the I5F mutant, but to a lesser extent. This is consistent with the preservation of heme deformation in the I5F crystal structure. However, the broadening of these peaks suggests that the heme is significantly more dynamic in the I5F mutant than in the I5L or WT *Tt* H-NOX proteins. In addition, the high-frequency skeletal markers, ν_3, ν_2, and ν_{10}, do not display changes in

dx.doi.org/10.1021/bi200788x | *Biochemistry* 2011, 50, 6832−6840

Table 2. Statistics for Data Collection, Processing, and Structure Refinement of the I5F Crystal Structure

	I5F *Tt* HNOX
space group	$P2_1$
cell dimensions	
a (Å)	44.6
b (Å)	67.1
c (Å)	66.4
β (deg)	92.0
wavelength (Å)	0.977408
temperature (K)	100
unique reflections	45085 (2223)
resolution range (Å)	50.00−1.67 (1.70−1.67)
average redundancy	3.7 (3.5)
completeness (%)[a]	100.0 (99.9)
$I/\sigma(I)$[a]	31.1 (2.2)
R_{sym} (%)[a,b]	4.2 (35.5)
no. of *Tt* HNOX molecules per asu	2
R_{cryst} (R_{free}) (%)[c]	19.7 (24.7)
average *B*-factor (Å^2)	
overall	30.9
protein	30.7
heme	17.9
waters	37.5
rms deviations	
bond lengths (Å)	0.008
bond angles (deg)	1.024
Ramachandran plot (%)[d]	
preferred	97.1 (330)
allowed	2.9 (10)
outliers	0 (0)

[a]The number in parentheses is for the highest resolution shell. [b]$R_{sym} = \sum^i_{hkl}|I^i_{(hkl)} - \langle I_{(hkl)}\rangle|/\sum_{hkl}\langle I_{(hkl)}\rangle$, where $I^i_{(hkl)}$ is the *i*th measured diffraction intensity and $\langle I_{(hkl)}\rangle$ is the mean of the intensity for the Miller index (*hkl*). [c]$R_{cryst} = \sum_{hkl}||F_o(hkl)| - |F_c(hkl)||/\sum_{hkl}|F_o(hkl)|$. $R_{free} = R_{cryst}$ for a test set of reflections (5%) not included in refinement. [d]Numbers in parentheses are the number of residues in each category.

frequency but exhibit peak broadening, further suggesting dynamic motion of the heme upon introduction of the I5F mutation. This dynamic motion of the heme is likely due to the interconversion of the F5 conformations that alter the orientation of the N-terminus and F78 conformations at the opposite end of the heme pocket.

The $Fe^{II}-O_2$ stretch shifted from 568 cm^{-1} in WT *Tt* H-NOX[9] to 562 cm^{-1} in the I5F mutant, which corresponds to a weakening of the $Fe^{II}-O_2$ bond. This decrease is consistent with the increased distance between the distal Y140 and the iron observed in the crystal structure. In addition, there was a decrease in the vibrational frequency of ν_4 in the I5F mutant spectra (by ~6 cm^{-1}) relative to the WT protein. This reduction corresponds to a decrease in electron density at the porphyrin core and a slightly larger macrocycle core size.[27] These results are also consistent with a more dynamic porphyrin as would be expected due to the I5F mutation, resulting in the protein N-terminus adopting two conformations and expanding the heme-binding cavity, accounting for the frequency change in ν_4 and the broadening of ν_3, ν_2, ν_{10}, and the heme deformation modes. The decreased $Fe^{II}-O_2$ stretching frequency is also consistent with the larger heme pocket and the increased distance between the iron and Y140 observed in the crystal structure. An increase in the Fe−Y140 distance is likely the cause of the increase in the O_2 dissociation rate for the I5F mutant as well as all of the double and triple mutants containing the I5F mutation. Without the strong hydrogen bond to trap the O_2 at the iron, O_2 dissociation and exit from the heme pocket is much more facile.

CONCLUSIONS

In summary, it is clear that the I5 position in *Tt* H-NOX is very important for both heme and protein conformational stability. This position is conserved as a medium-sized (V, I, L), hydrophic amino acid, further emphasizing the role of this residue in controlling protein structure and ligand affinity. Although the conservative I5L mutant shows modest changes, the I5F mutation results in large decreases in O_2 affinity due to extremely rapid O_2 association and dissociation rates (Table 1). In contrast, mutation of I5 to alanine results in a mutant with a decreased O_2 dissociation rate, suggesting an increased O_2 affinity (k_{off} = 0.82 s^{-1}). Therefore, the contacts made by the amino acid at position 5 are likely required for tuning the ligand affinity in H-NOX domains. In addition to the single mutants, the I5F mutation synergizes with the previously described I75F and L144F mutations, resulting in proteins with significantly faster O_2 association and dissociation rates, as compared to WT *Tt* H-NOX. Resonance Raman and X-ray crystallographic studies have found that the I5F mutation also results in multiple conformations of the N-terminus and increased flexibility of the heme, suggesting that this residue is a key factor in maintaining structural rigidity. This rigidity may be important for signaling as it has previously been found that N-terminal movement of an H-NOX domain from *S. oneidensis* affects the activity of its cognate kinase.[31] Conformational stability is likely also a method by which the H-NOX family can ensure high affinity ligand binding, even at the elevated temperatures (70−90 °C) at which the *T. tengcongensis* bacterium lives. These results provide additional evidence for the heme pocket of *Tt* H-NOX being tightly packed to exquisitely tune ligand−binding properties. In addition, this work further emphasizes the myriad factors that control ligand affinity within heme proteins as well as the extent to which these factors are interlinked. An improved understanding of the interplay between the factors controlling ligand affinity should allow for the design of novel heme proteins that can be used for a variety of sensing and delivery applications in biotechnology and medicine. Engineered flexibility may be a novel strategy for controlling O_2 affinity and binding kinetics to rationally tune the affinity of heme proteins.

ASSOCIATED CONTENT

Supporting Information

Figure S1 (comparison of Mb and *Tt* H-NOX heme pockets), Figure S2 (resonance Raman spectra of various steric bulk mutants), Figure S3 (composite omit density of the loop 27−47), Figure S4 (composite omit density and the two comformations of F78 in the heme pocket), Table S1 (electronic absorption spectra), Table S2 (NO dissociation rates), and Table S3 (RR skeletal markers). This material is available free of charge via the Internet at http://pubs.acs.org.

Accession Codes

The coordinates have been deposited in the RCSB Protein Data Bank as entry 3SJ5.

AUTHOR INFORMATION

Corresponding Author

*Tel: 510-666-2763. Fax: 510-666-2765. E-mail: marletta@berkeley.edu.

Present Address

[§]Physical Biosciences Division, Lawrence Berkeley National Laboratory, 1 Cyclotron Road, Mail Stop 66R0200, Berkeley, CA 94720.

Author Contributions

[‖]These authors contributed equally to this work.

Funding

Financial support was provided by NIH Grant GM070671 (M.A.M.), the Rogers Family Fund (M.A.M.), and NIH National Heart Lung and Blood Institute Award F32HL090174 (E.E.W.).

ACKNOWLEDGMENTS

The authors are grateful to Charlotte Whited, Professor Harry Gray, Dr. Jay Winkler, and the Beckman Institute Laser Resource Center at the California Institute of Technology for assistance with O_2 association rate measurements, Professor John Kuriyan for use of crystallography equipment, Professor Elizabeth Boon for acquisition of the I5L and I5A O_2 dissociation rates, Mark Herzik for assistance with protein crystallography, Michael Winter for helpful discussions, and members of the Marletta laboratory for critical reading of this manuscript. The crystal data were collected at the Advanced Light Source in Berkeley, CA at Beamline 5.0.1, which is supported by the DOE Contract DE-AC02-05CH11231.

ABBREVIATIONS

H-NOX, *H*eme *N*itric oxide and/or *OX*ygen binding domain; myoglobin, Mb; hemoglobin, Hb; *Tt*, *Thermoanaerobacter tengcongensis*; rmsd, root-mean-square deviation; RR, resonance Raman spectroscopy; WT, wild type; I, isoleucine; L, leucine; F, phenylalanine.

REFERENCES

(1) Springer, B. A., Sligar, S. G., Olson, J. S., and Phillips, G. N. (1994) Mechanisms of Ligand Recognition in Myoglobin. *Chem. Rev. 94*, 699−714.

(2) Dou, Y., Maillett, D. H., Eich, R. F., and Olson, J. S. (2002) Myoglobin as a model system for designing heme protein based blood substitutes. *Biophys. Chem. 98*, 127−148.

(3) Antonini, E., and Brunori, M. (1971) *Hemoglobin and Myoglobin in Their Reactions with Ligands*, North-Holland Pub. Co., Amsterdam.

(4) Lukin, J. A., and Ho, C. (2004) The structure--function relationship of hemoglobin in solution at atomic resolution. *Chem. Rev. 104*, 1219−1230.

(5) Olson, J. S., and Phillips, G. N. Jr. (1997) Myoglobin discriminates between O_2, NO, and CO by electrostatic interactions with the bound ligand. *J. Biol. Inorg. Chem. 2*, 544−552.

(6) Olson, J. S., Soman, J., and Phillips, G. N. Jr. (2007) Ligand pathways in myoglobin: a review of Trp cavity mutations. *IUBMB Life 59*, 552−562.

(7) Capece, L., Marti, M. A., Crespo, A., Doctorovich, F., and Estrin, D. A. (2006) Heme protein oxygen affinity regulation exerted by proximal effects. *J. Am. Chem. Soc. 128*, 12455−12461.

(8) Iyer, L. M., Anantharaman, V., and Aravind, L. (2003) Ancient conserved domains shared by animal soluble guanylyl cyclases and bacterial signaling proteins. *BMC Genomics 4*, 5.

(9) Karow, D. S., Pan, D., Tran, R., Pellicena, P., Presley, A., Mathies, R. A., and Marletta, M. A. (2004) Spectroscopic characterization of the soluble guanylate cyclase-like heme domains from *Vibrio cholerae* and *Thermoanaerobacter tengcongensis*. *Biochemistry 43*, 10203−10211.

(10) Derbyshire, E. R., and Marletta, M. A. (2009) Biochemistry of soluble guanylate cyclase. *Handb. Exp. Pharmacol.*, 17−31.

(11) Boon, E. M., Huang, S. H., and Marletta, M. A. (2005) A molecular basis for NO selectivity in soluble guanylate cyclase. *Nat. Chem. Biol. 1*, 53−59.

(12) Nioche, P., Berka, V., Vipond, J., Minton, N., Tsai, A. L., and Raman, C. S. (2004) Femtomolar sensitivity of a NO sensor from *Clostridium botulinum*. *Science 306*, 1550−1553.

(13) Price, M. S., Chao, L. Y., and Marletta, M. A. (2007) *Shewanella oneidensis* MR-1 H-NOX regulation of a histidine kinase by nitric oxide. *Biochemistry 46*, 13677−13683.

(14) Ma, X., Sayed, N., Beuve, A., and van den Akker, F. (2007) NO and CO differentially activate soluble guanylyl cyclase via a heme pivot-bend mechanism. *EMBO J. 26*, 578−588.

(15) Pellicena, P., Karow, D. S., Boon, E. M., Marletta, M. A., and Kuriyan, J. (2004) Crystal structure of an oxygen-binding heme domain related to soluble guanylate cyclases. *Proc. Natl. Acad. Sci. U. S. A. 101*, 12854−12859.

(16) Olea, C., Boon, E. M., Pellicena, P., Kuriyan, J., and Marletta, M. A. (2008) Probing the function of heme distortion in the H-NOX family. *ACS Chem. Biol. 3*, 703−710.

(17) Olea, C. Jr., Kuriyan, J., and Marletta, M. A. (2010) Modulating heme redox potential through protein-induced porphyrin distortion. *J. Am. Chem. Soc. 132*, 12794−12795.

(18) Weinert, E. E., Plate, L., Whited, C. A., Olea, C. Jr., and Marletta, M. A. (2010) Determinants of ligand affinity and heme reactivity in H-NOX domains. *Angew. Chem., Int. Ed. 49*, 720−723.

(19) Martin, E., Berka, V., Bogatenkova, E., Murad, F., and Tsai, A.-L. (2006) Ligand Selectivity of Soluble Guanylyl Cyclase: Effect of the Hydrogen-Bonding Tyrosine in the Distal Heme Pocket on Binding of Oxygen, Nitric Oxide, and Carbon Monoxide. *J. Biol. Chem. 281*, 27836−27845.

(20) Derbyshire, E. R., Deng, S., and Marletta, M. A. (2010) Incorporation of tyrosine and glutamine residues into the soluble guanylate cyclase heme distal pocket alters NO and O2 binding. *J. Biol. Chem. 285*, 17471−17478.

(21) Dmochowski, I. J., Winkler, J. R., and Gray, H. B. (2000) Enantiomeric discrimination of Ru-substrates by cytochrome P450cam. *J. Inorg. Biochem. 81*, 221−228.

(22) Otwinowski, Z., and Minor, W. (1997) Processing of X-ray diffraction data collected in oscillation mode. *Macromol. Crystallogr., Part A 276*, 307−326.

(23) Storoni, L. C., McCoy, A. J., and Read, R. J. (2004) Likelihood-enhanced fast rotation functions. *Acta Crystallogr. D60*, 432−438.

(24) Adams, P. D., Afonine, P. V., Bunkoczi, G., Chen, V. B., Davis, I. W., Echols, N., Headd, J. J., Hung, L. W., Kapral, G. J., Grosse-Kunstleve, R. W., McCoy, A. J., Moriarty, N. W., Oeffner, R., Read, R. J., Richardson, D. C., Richardson, J. S., Terwilliger, T. C., and Zwart, P. H. (2010) PHENIX: a comprehensive Python-based system for macromolecular structure solution. *Acta Crystallogr., Sect. D: Biol. Crystallogr. 66*, 213−221.

(25) Emsley, P., and Crowtan, K. (2004) Coot: model-building tools for molecular graphics. *Acta Crystallogr. D60*, 2126−2132.

(26) Tran, R., Boon, E. M., Marletta, M. A., and Mathies, R. A. (2009) Resonance Raman spectra of an O_2-binding H-NOX domain reveal heme relaxation upon mutation. *Biochemistry 48*, 8568−8577.

(27) Spiro, T. G., and Li, X. Y. (1988) Resonance Raman Spectroscopy of Metalloporphyrins, in *Biological Applications of Raman Spectroscopy: Resonance Raman Spectra of Heme and Metalloproteins* (Spiro, T. G., Ed.), pp 1−37, John Wiley & Sons, New York.

(28) Huang, Q., Medforth, C. J., and Schweitzer-Stenner, R. (2005) Nonplanar heme deformations and excited state displacements in nickel porphyrins detected by Raman spectroscopy at soret excitation. *J. Phys. Chem. A 109*, 10493−10502.

(29) Shelnutt, J. A., Song, X. Z., Ma, J. G., Jia, S. L., Jentzen, W., and Medforth, C. J. (1998) Nonplanar porphyrins and their significance in proteins. *Chem. Soc. Rev. 27*, 31−41.

(30) Spiro, T. G., Stong, J. D., and Stein, P. (1979) Porphyrin Core Expansion and Doming in Heme-Proteins - New Evidence from Resonance Raman-Spectra of 6-Coordinate High-Spin Iron(III) Hemes. *J. Am. Chem. Soc. 101*, 2648−2655.

(31) Erbil, W. K., Price, M. S., Wemmer, D. E., and Marletta, M. A. (2009) A structural basis for H-NOX signaling in Shewanella oneidensis by trapping a histidine kinase inhibitory conformation. *Proc. Natl. Acad. Sci. U. S. A. 106*, 19753−19760.